Domain wall free polar structure enhanced photodegradation activity in nanoscale ferroelectric $Ba_xSr_{1-x}TiO_3$

Yaqiong Wang, Man Zhang, Jianguo Liu, Haibin Zhang, Feng Li, Chiao-Wei Tseng, Bin Yang, Graham Smith, Jiwei Zhai, Zhen Zhang, Steve Dunn, Haixue Yan**

Dr. Yaqiong Wang, Dr Haixue Yan, Man Zhang

School of Engineering and Materials Science

Queen Mary University of London

Mile End Road, London, E1 4NS, UK

E-mail: h.x.yan@qmul.ac.uk

Dr. Yaqiong Wang, Prof. Steve Dunn

School of Engineering

London South Bank University

103 Borough Road, London SE1 0AA UK
E-mail: dunns4@lsbu.ac.uk

Prof. Jianguo Liu

School of Environment

Tsinghua University

1 Qinghuayuan, Beijing, 100084, China

Prof. Haibin Zhang

Innovation Research Team for Advanced Ceramics

Institute of Nuclear Physics and Chemistry

China Academy of Engineering Physics

Mianyang, 621900, China

Dr. Feng Li, Prof. Jiwei Zhai

Key Laboratory of Advanced Civil Engineering Materials of Ministry of Education

Functional Materials Research Laboratory

School of Materials Science & Engineering

Tongji University

4800 Caoan Road, Shanghai 201804, China

Dr. Chiao-Wei Tseng, Prof. Zhen Zhang

Division of Solid-State Electronics

Department of Electrical Engineering

Uppsala University
Lagerhyddsvagen 1, Uppsala, Sweden

Dr. Bin Yang, Prof. Graham Smith
Faculty of Science and Engineering

University of Chester

Thornton Science Park, CH2 4NU, UK

Keywords: ferroelectrics, domain wall free, photocatalysis, barium strontium titanates

Abstract

Ferroelectric materials exhibit anomalous behavior due to the presence of domains and domain walls which are related to the spontaneous polarization inherent in the crystal structure. Control of ferroelectric domains and domain walls has been used to enhance device performances in ultrasound, pyroelectric detectors and photovoltaic systems with renewed interest in nanostructuring for energy applications. It is also known that the ferroelectric including domain walls can double photocatalytic rate and increase carrier lifetime from μs to ms[1] However, there remains a lack of understanding on the different contributions of the domain and domain walls to photo-catalytic activities. Herein it is found, by comparing samples of nanostructured $Ba_xSr_{1-x}TiO_3$ with and without a polar domain, that the material with polar domains has a faster reaction rate ($k=0.18\ min^{-1}$) than the non-polar one ($k = 0.11\ min^{-1}$). It is further revealed that the observed enhanced photoactivity of perovskite ferroelectric materials stems from the inherent polarization of the domain instead of domain walls. Here, the new understanding of

the underlying physics of materials with a spontaneous dipole opens a door to enhance the performance of light induced energy harvesting systems.

Introduction

Questions arising from the fundamental physics related to domain stability have been evident for ferroelectric materials since ferroelectric domains were first reported.[2] This interest extends to the aspects of domain wall motion, influence of domain on charge separation and the interactions of dipoles as the domain size approaches nanoscale and ultimately the unit cell. Computational studies performed on the surfaces restructuring of ferroelectric during a phase change show the advantages of using polar materials to drive surface chemical reactions over a polydomain material.[3] To date experimental and computational studies have mainly focused on polycrystalline, or polydomain ferroelectric single crystals. These studies have largely shown that the ferroelectric material can enhance photocatalytic activity and energy conversion efficiency in photovoltaic devices.[4] The development of organic halide perovskites as sensitizers in photovoltaic devices has brought the concept of enhanced photo-carrier separation effect into sharp focus for polydomain polar materials.[5] The growing evidence of polar nanodomains in lead halide systems further confirms the inherent influence of polar materials in light harvesting.[6] The studies conducted on metal halide systems is also supported by previous work on metal oxide materials showing enhanced photon induced performance.[7] Despite these studies, a fundamental question still remains to be answered: are these ferroelectric enhanced device performance resulted from the domain wall, or from the inherent spontaneous polarization in the domains of the ferroelectric material.

Domain walls have significant influence on the local surface potential and surface free energy[8, 9] and may influence the surface chemistry in an analogous manner to the anomalous photocatalytic field.[10] When assessing photovoltaic and photocatalytic performance of polar materials the contribution from both domain and domain walls should be considered. Atomic level structures of domain wall were successfully characterized using advanced aberration-corrected transmission electron microscope (STEM) in some ferroelectrics, which shows that the polarization in DWs is smaller than that in domains.[11] Furthermore, complications also arise to understand the domain structure in nanostructured systems. Tools such as X-ray diffraction (XRD) can give useful insights but XRD is typically inferring the polar/non-polar structure of materials from the unit cell by characterizing their crystallography. It often fails on nanosized ferroelectrics due to the lack of long-range coherency of distortions.[12, 13] Techniques such as transmission electron microscopy (TEM), piezo-force microscopy (PFM) and Raman, have proved the existence of spontaneous polarization in ferroelectric particles at the unit cell scale.[14] These complications in interpreting analytical data make it difficult to fully understand the domain structure of small ferroelectric systems, and therefore any influence on the behavior of photo induced carriers.

In order to investigate whether domain walls are the dominant cause of the enhanced carrier separation as well the associated photocatalytic performance improvement, two single-crystalline BST nanoparticles were prepared: $Ba_{0.8}Sr_{0.2}TiO_3$ (single-domain without domain walls T_c 77 °C) and $Ba_{0.2}Sr_{0.8}TiO_3$ (no domain T_c -148 °C).[15] The polar, non-polar nature of the structures at room temperature has been confirmed by Raman, differential scanning calorimetry (DSC), microscopy and XRD analysis. By measuring their photocatalytic decomposition of a dye molecule, we confirm that our nanoscale single crystalline single

domain samples (without domain walls) still enhance the carrier separation with their inherent dipole. This proves that it is not necessary for a domain wall to be present for efficient carrier separation and that the dipole of the ferroelectric drives mobile carrier separation.

The phase composition of the as-produced samples was analyzed using XRD. The 20°-70° 2θ patterns obtained are shown in **Figure 1**a. The structure is single phase cubic. As expected, no obvious peak splitting was observed at 2θ = 45° for $Ba_{0.8}Sr_{0.2}TiO_3$ in the tetragonal phase below the Curie point (T_c). This is believed to be related with the formation of the single-domain-single-grain structures with decreased spontaneous distortion.[12] The transition at T_c from the cubic to the ferroelectric tetragonal structure is accompanied by spontaneous strain and a small volume increase. In micro meter sized grains which show single grain multi domain structures, the change of lattice dimensions and the internal stresses produced by the volume increase can be minimized by domain walls. In nano meter sized grains which show single grain single domain structures, domains walls are absent. Consequently, the resulting stresses cannot be relieved by domain walls. On average, the stresses are of compressive because of the volume increase, thus tending to suppress the spontaneous distortion, which results in a reduced c/a ratio. This makes it difficult to distinguished between polar and non-polar materials in an XRD pattern.[16]

The two BST samples have similar particles sizes measured using BET as shown in Table S1. The average particle size of $Ba_{0.8}Sr_{0.2}TiO_3$ was measured as 70.8 nm, for the $Ba_{0.2}Sr_{0.8}TiO_3$ sample it was 65.2 nm as measured from 100 particles imaged using SEM. The BET surface areas are 7.3904 m^2/g for $Ba_{0.8}Sr_{0.2}TiO_3$ and 7.9646 m^2/g for $Ba_{0.2}Sr_{0.8}TiO_3$ sample. The BET

surface area represents a difference of 7% extra surface area for the non-polar material. This material has the higher surface area but the lower photoactivity.

Further investigation of the microstructure of $Ba_{0.8}Sr_{0.2}TiO_3$ and $Ba_{0.2}Sr_{0.8}TiO_3$ was performed using TEM, shown in **Figure 2.** Analysis of the electron diffraction patterns (Figure 2b, e) for the nanoparticles identifies them as single-crystals. It is noteworthy that the TEM generated diffraction patterns also show a cubic structure for both samples. This is consistent with XRD results and suggests the requirement of suitable techniques to determine whether this nanoscale sample is polar or not. $Ba_{0.8}Sr_{0.2}TiO_3$, which is expected to have a spontaneous polarization, does not have any domain wall or other internal features in the TEM images. The single-domain structure of $Ba_{0.8}Sr_{0.2}TiO_3$ was further evidenced by the DSC measurements as detailed in **Figure S1**. The endothermic peak representing the tetragonal to cubic phase is not present in small-sized $Ba_{0.8}Sr_{0.2}TiO_3$ powders. The absence of this peak indicates that there has been a multi- to single-domain transformation in the sample.[12]

The high sensitivity of the Raman spectroscopy to short-range distortions such as microstructural defects and symmetry changes[12] makes it a suitable tool to study the polar nature of nanoscale ferroelectric materials. Raman spectra of $Ba_{0.8}Sr_{0.2}TiO_3$ and $Ba_{0.2}Sr_{0.8}TiO_3$ collected at room temperature are shown in Figure 2c, f. The characteristic peaks of ferroelectric order found in the spectrum of $Ba_{0.8}Sr_{0.2}TiO_3$ at 302 cm^{-1} and 722 cm^{-1} indicate the tetragonal phase and polar nature of the sample. The peaks centered at 234 cm^{-1} and 516 cm^{-1} have been attributed to disorder of titanium.[13] By contrast the spectrum for $Ba_{0.2}Sr_{0.8}TiO_3$ shows no peaks related to ferroelectric order. The Raman peaks found for $Ba_{0.2}Sr_{0.8}TiO_3$ are analogous to those reported for nanocrystalline $SrTiO_3$, a paraelectric materials lacking a ferroelectric response.[17]

Temperature-dependent Raman spectra of the $Ba_{0.8}Sr_{0.2}TiO_3$ sample were obtained to reveal its phase transformation with temperature changing through the Curie point. The information is given in **Figure S2.** The two peaks at 302 cm^{-1} and 722 cm^{-1} vanish when temperature increased from 25 °C to 200 °C, which further demonstrates polar nature of the sample.

Figure 3a shows optical properties of the x=0.2 and x=0.8 samples characterized by UV-vis diffuse reflectance spectroscopy. The band gaps of the samples have been estimated from the Tauc plot, shown in Figure 3b. The band gaps of $Ba_{0.8}Sr_{0.2}TiO_3$ and $Ba_{0.2}Sr_{0.8}TiO_3$ are both estimated to be 3.24 eV. This is to be expected as the Ti and O systems in the lattice most strongly influence the band gap and allows a comparison of the photoactivity based on similar light absorption characteristics. We, therefore, provide compelling evidence that we have produced two samples that differ substantially in their polar nature but are similar in other properties, such as band structure, surface area and size (SEM, TEM data).

Figure 3c and Figure 3d give the UV-vis absorption spectra of RhB dye solutions as a function of illumination time for the two photocatalysts. The maximum absorption peak for RhB was located at 554 nm with absorption by the dye, and it decreased with the illumination time. The absorbance at zero time at λ_{max} (554 nm) was taken as C_0. The concentrations of other samples, taken as C_i, are determined according to the absorption measurement at 540 nm where absorbance is proportional to the concentration. The percentage of photodecolourisation X was calculated using Equation (1):

$$X\ (\%) = (1-C_i/C_0) * 100 \qquad (1)$$

The photodecolourisation curves of RhB of the two $Ba_xSr_{1-x}TiO_3$ samples are shown in Figure 3e. It can be seen that $Ba_{0.8}Sr_{0.2}TiO_3$ shows an enhanced efficiency in RhB decolourisation over $Ba_{0.2}Sr_{0.8}TiO_3$. The kinetics of photocatalytic decolourisation of RhB follows the Langmuir-Hinshelwood model which can be simplified to a pseudo-first-order equation. Integration gives the relationship[18]:

$$\ln\left(\frac{C_i}{C_0}\right) = k_{obs}t \qquad (2)$$

where k_{obs} is the reaction rate obtained from the slope of ln (C_0/C) vs t. The derived k_{obs} of the degradation process is shown in **Table 1**. A comparison of rate constants in Table 1 shows that the polar $Ba_{0.8}Sr_{0.2}TiO_3$ has a faster reaction rate than the non-polar $Ba_{0.2}Sr_{0.8}TiO_3$. Our evaluation of the other physical properties (surface area, band gap) shows that these vary by less than k_{obs}. The two $Ba_xSr_{1-x}TiO_3$ materials possess close surface area and the same band gap values. Moreover, $Ba_{0.8}Sr_{0.2}TiO_3$ and $Ba_{0.2}Sr_{0.8}TiO_3$ are single-grain-single-domain and non-domain structure, respectively. Our materials, therefore, allow for a comparison of spontaneous polarization effect without a contribution from domain walls. Thus, the enhanced photocatalytic performance of the $Ba_{0.8}Sr_{0.2}TiO_3$ can be attributed to the effect from its polar structure in the absence of domain walls. By the way, domain walls normally show low polarization values[9], which suggests that the contribution of domain walls in terms of working as an electrical field to separate photo carries (holes and electrons) is lower than that of domains.

Figure 4 provides a schematic of the energy level diagrams for the $Ba_xSr_{1-x}TiO_3$ samples. In $Ba_{0.8}Sr_{0.2}TiO_3$ which has the polar structure, band bending at the surface occurs due to the spontaneous polarization induced charge screening as that has been widely reported in ferroelectrics[8, 19]. The spontaneous polarization P, pointing from the bounded negative charges

to positive charges, creates an internal electric field which has the opposite direction to it and drives the free carries within the material to two sides of the surface. Accumulation of these carries causes upward and downward band bending at the surface respectively. This band bending situation happen in an ambient environment and is presented in Figure 4a. Compared to $Ba_{0.8}Sr_{0.2}TiO_3$, the non-polar $Ba_{0.2}Sr_{0.8}TiO_3$ exhibits no internally driven band bending, as shown in Figure 4b. When the $Ba_xSr_{1-x}TiO_3$ samples contact an aqueous solution band bending occurs due to migration of mobile species across the semi-conductor liquid interface[20], the band bending situation is presented in Figure 4c and 4d. This process usually causes upward band bending for n type materials. The higher permittivity of polar structure is also useful to improve photocatalytic preference which is consistent with the work in bulk ceramics.[21] In the polar material the polarisation driven band bending enhances photocatalytic rate.

Conclusions

In conclusion, we have produced nanometer sized $Ba_xSr_{1-x}TiO_3$ single crystals through a molten-salt method. The material $Ba_{0.8}Sr_{0.2}TiO_3$ exhibits a single-crystal-single-domain morphology. The polar nature is dependent on the Currie point of the produced particles. Influence of polar nature on the photocatalytic activities of the nanoparticles was evaluated through photocatalytic mineralization of RhB. These results indicate that the decolourisation rate was enhanced when the material with spontaneous polarization was used. We attribute this enhanced reaction rate to the separation of carriers due to the internal electric field present in polar structured ferroelectrics. Our results provide evidence that the internal electric field within a single domain can enhance carrier separation and increase photocatalytic activities.

Supporting Information

Supporting Information is available from the Wiley Online Library or from the author.

Acknowledgements

The authors would like to acknowledge the Chinese Scholarship Council for supporting this work. Financial supports from LSBU, and the Wallenberg Academy Fellow Program (for Zhen Zhang) are acknowledged.

Received: ((will be filled in by the editorial staff))

Revised: ((will be filled in by the editorial staff))

Published online: ((will be filled in by the editorial staff))

References

[1] M. R. Morris, S. R. Pendlebury, J. Hong, S. Dunn, J. R. Durrant, *Adv. Mater.* **2016**, 7123.

[2] S. Li, J. Eastman, Z. Li, C. Foster, R. Newnham, L. Cross, *Phys. Lett. A* **1996**, *212*, 341.

[3] A. Kakekhani, S. Ismail-Beigi, *J. Mater. Chem. A* **2016**, *4*, 5235.

[4] L. Pan, S. Sun, Y. Chen, P. Wang, J. Wang, X. Zhang, J.-J. Zou, Z. L. Wang, *Advanced Energy Materials* **2020**, *10*, 2000214; J. Chen, H. Lu, H.-J. Liu, Y.-H. Chu, S. Dunn, K. Ostrikov, A. Gruverman, N. Valanoor, *Applied Physics Letters* **2013**, *102*, 182904; Y. Cui, S. M. Goldup, S. Dunn, *RSC Advances* **2015**, *5*, 30372; N. V. Burbure, P. A. Salvador, G. S. Rohrer, *Chem. Mater.* **2010**, *22*, 5831.

[5] M. Ahmadi, L. Collins, A. Puretzky, J. Zhang, J. K. Keum, W. Lu, I. Ivanov, S. V. Kalinin, B. Hu, *Adv. Mater.* **2018**, *30*, 1705298; D. Kim, J. S. Yun, P. Sharma, J. Kim, A. M. Soufiani, S. Huang, M. A. Green, A. W. Ho-Baillie, J. Seidel, *Nat. Commun.* **2019**, *10*, 444.

[6] H. Röhm, T. Leonhard, M. J. Hoffmann, A. Colsmann, *Energy Environ. Sci.* **2017**, *10*, 950; K. Miyata, X.-Y. Zhu, *Nat. Mater.* **2018**, *17*, 379.

[7] D. Meggiolaro, F. Ambrosio, E. Mosconi, A. Mahata, F. De Angelis, *Advanced Energy Materials* **2020**, *10*, 1902748.

[8] S. V. Kalinin, D. A. Bonnell, T. Alvarez, X. Lei, Z. Hu, J. Ferris, Q. Zhang, S. Dunn, *Nano Lett.* **2002**, *2*, 589.

[9] G. Nataf, M. Guennou, J. Kreisel, P. Hicher, R. Haumont, O. Aktas, E. Salje, L. Tortech, C. Mathieu, D. Martinotti, *Phys. Rev. Mater.* **2017**, *1*, 074410.

[10] B. I. Sturman, V. M. Fridkin, *The Photovoltaic and Photorefractive Effects in Noncentrosymmetric Materials*, Vol. 8, Gordon and Breach Science Publisher, Philadelphia 1992.

[11] C.-L. Jia, S.-B. Mi, K. Urban, I. Vrejoiu, M. Alexe, D. Hesse, *Nat. Mater.* **2008**, *7*, 57; C. T. Nelson, B. Winchester, Y. Zhang, S.-J. Kim, A. Melville, C. Adamo, C. M. Folkman, S.-H. Baek, C.-B. Eom, D. G. Schlom, L.-Q. Chen, X. Pan, *Nano Lett.* **2011**, *11*, 828.

[12] M. H. Frey, D. A. Payne, *Phys. Rev. B* **1996**, *54*, 3158.

[13] M. B. Smith, K. Page, T. Siegrist, P. L. Redmond, E. C. Walter, R. Seshadri, L. E. Brus, M. L. Steigerwald, *J. Am. Chem. Soc.* **2008**, *130*, 6955.

[14] M. J. Polking, M.-G. Han, A. Yourdkhani, V. Petkov, C. F. Kisielowski, V. V. Volkov, Y. Zhu, G. Caruntu, A. Paul Alivisatos, R. Ramesh, *Nat. Mater.* **2012**, *11*, 700.

[15] L. Zhou, P. Vilarinho, J. Baptista, *J. Eur. Ceram. Soc.* **1999**, *19*, 2015; J. Nowotny, M. Rekas, *Key Eng. Mater.* **1992**, *66-67*, 45.

[16] Z. Zhao, V. Buscaglia, M. Viviani, M. T. Buscaglia, L. Mitoseriu, A. Testino, M. Nygren, M. Johnsson, P. Nanni, *Phys. Rev. B* **2004**, *70*, 024107.

[17] F. A. Rabuffetti, H.-S. Kim, J. A. Enterkin, Y. Wang, C. H. Lanier, L. D. Marks, K. R. Poeppelmeier, P. C. Stair, *Chem. Mater.* **2008**, *20*, 5628.

[18] J.-M. Herrmann, *Catal. Today* **1999**, *53*, 115.

[19] S. Dunn, P. M. Jones, D. E. Gallardo, *J. Am. Chem. Soc.* **2007**, *129*, 8724.

[20] L. Li, P. A. Salvador, G. S. Rohrer, *Nanoscale* **2014**, *6*, 24.

[21] A. Bhardwaj, N. V. Burbure, G. S. Rohrer, *J. Am. Ceram. Soc.* **2010**, *93*, 4129.

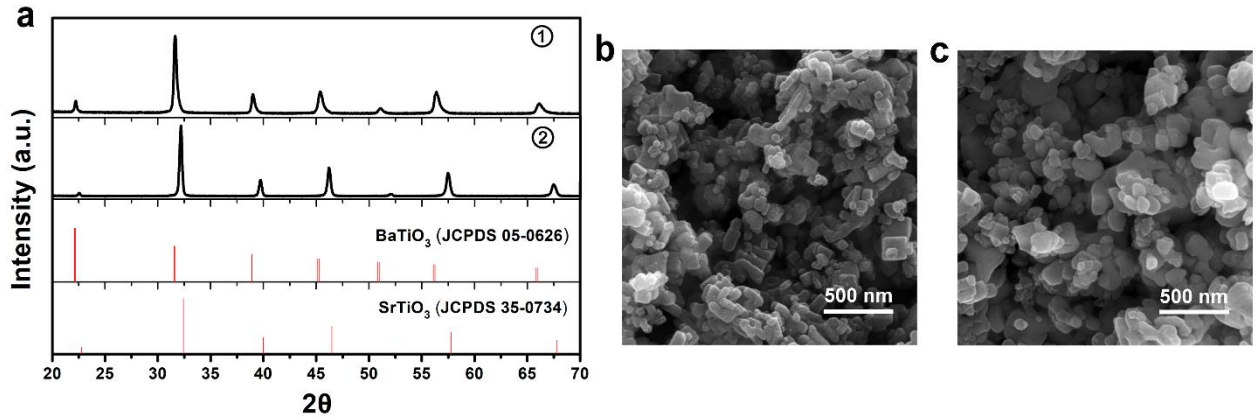

Figure 1. Phase and morphology of BST nanocrystals. (a) XRD pattern of ① $Ba_{0.8}Sr_{0.2}TiO_3$ ② $Ba_{0.2}Sr_{0.8}TiO_3$. (b) SEM micrograph of $Ba_{0.8}Sr_{0.2}TiO_3$ and (c) SEM micrograph of $Ba_{0.2}Sr_{0.8}TiO_3$.

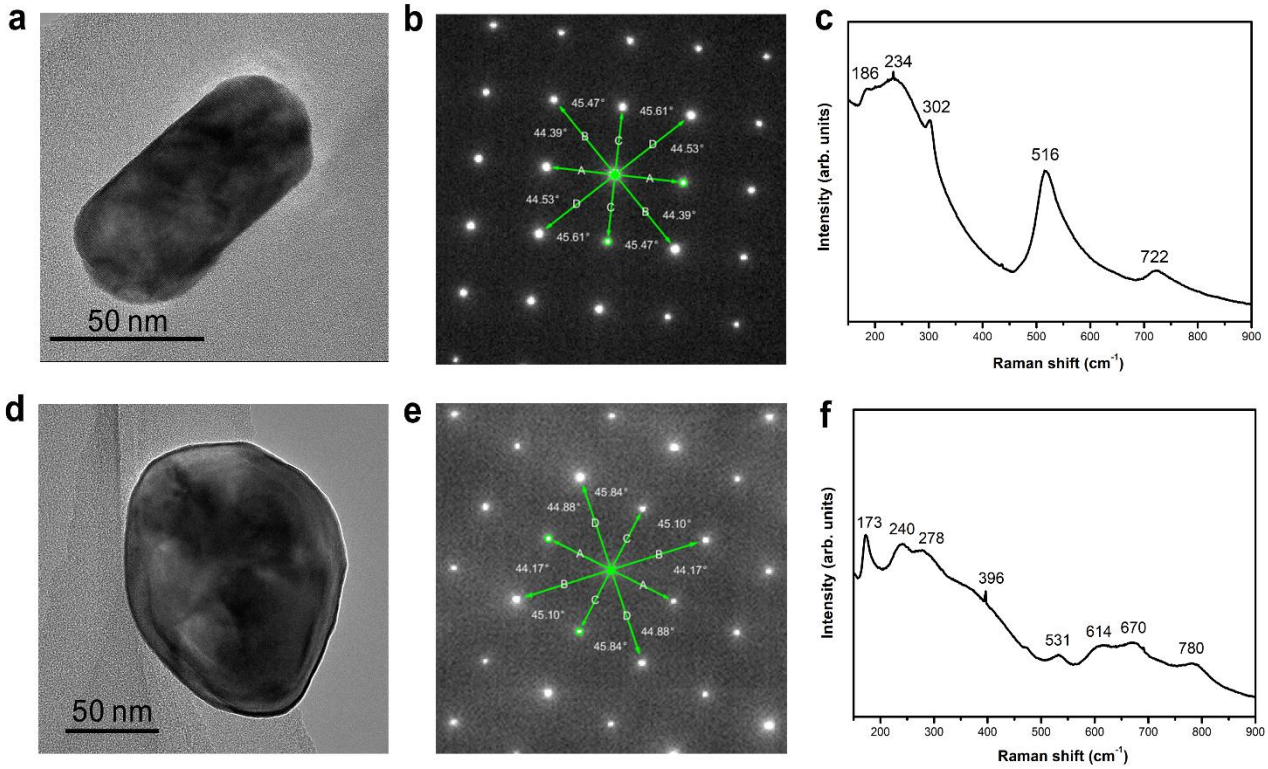

Figure 2. Microstructure and lattice dynamics characterisation of BST. (a) and (d) TEM image of a typical $Ba_{0.8}Sr_{0.2}TiO_3$ crystal and a $Ba_{0.2}Sr_{0.8}TiO_3$ crystal. (b) and (e) Electron diffraction patterns of $Ba_{0.8}Sr_{0.2}TiO_3$ and $Ba_{0.2}Sr_{0.8}TiO_3$, respectively. (c) and (f) Room-temperature Raman spectra of $Ba_{0.8}Sr_{0.2}TiO_3$ and $Ba_{0.2}Sr_{0.8}TiO_3$.

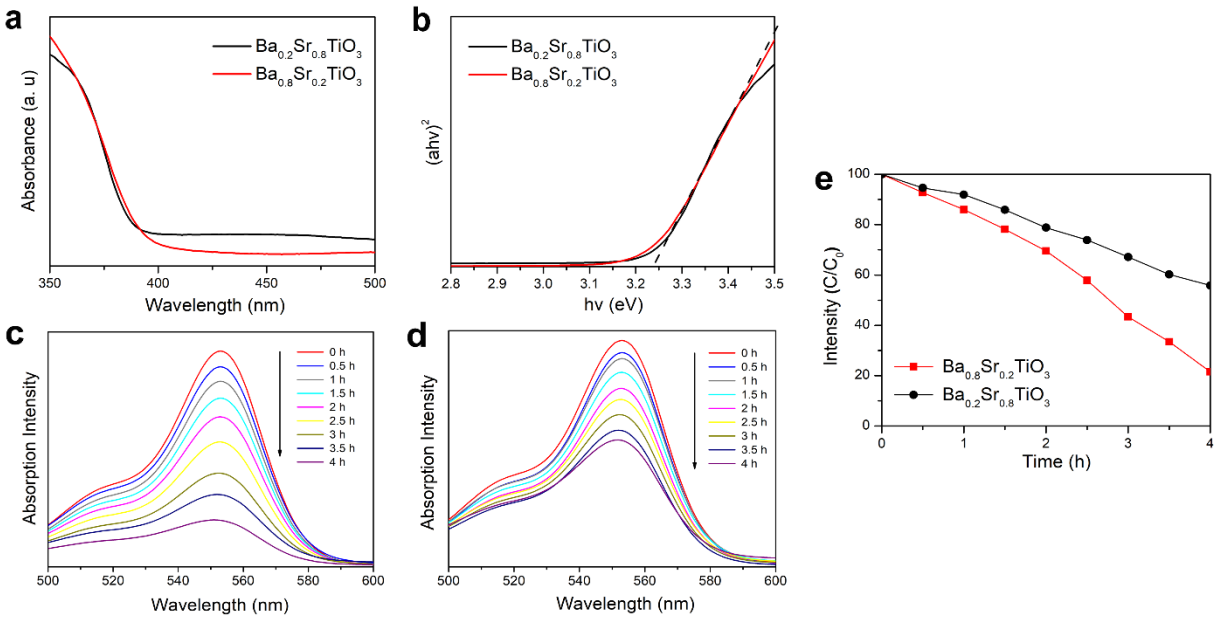

Figure 3. Optical property and photoactivity characterisation of BST. (a) UV-vis spectra of $Ba_{0.8}Sr_{0.2}TiO_3$ and $Ba_{0.2}Sr_{0.8}TiO_3$. (b) Tauc plots of the nanocrystals derived from a to determine the optical bandgaps. (c) and (d) UV-vis absorption spectra of RhB dye solutions obtained at different degradation time with $Ba_{0.8}Sr_{0.2}TiO_3$ and $Ba_{0.2}Sr_{0.8}TiO_3$. (e) Degradation of Rh B with the two catalysts under solar simulator to assess their photoactivity.

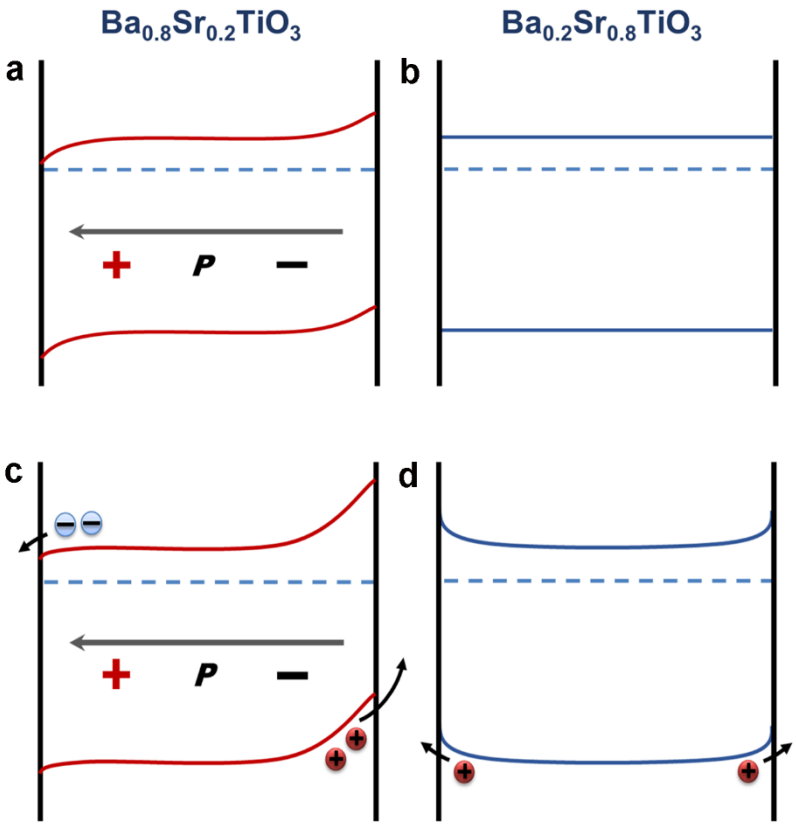

Figure 4. Schematic representation of the energy level diagrams for $Ba_{0.8}Sr_{0.2}TiO_3$ and $Ba_{0.2}Sr_{0.8}TiO_3$ in ambient (a, b) and aqueous solution (c, d). The polar $Ba_{0.8}Sr_{0.2}TiO_3$ has band bending in ambient condition due to the spontaneous polarisation induced screening effect, with upward band bending occurs on the surface of C^- domain and downward band bending occurs on the surface of C^+ domain (a). The non-polar $Ba_{0.2}Sr_{0.8}TiO_3$ in ambient condition has no band bending (b). When in contact with aqueous solution and energy equilibrium achieved, the upward band bending increases and downward band bending decreases in $Ba_{0.8}Sr_{0.2}TiO_3$ (c). $Ba_{0.2}Sr_{0.8}TiO_3$ behaves as a typical n type semiconductor and shows upward band bending in aqueous solution (d). ***P*** is the spontaneous polarization, which points from the negative charges to the positive charges.

The table of contents

By comparing the performance of domain wall free polar material with a non-polar material, compelling evidence has been provided that there is no need for a domain wall to be present for increased photodegradation activity in a perovskite ferroelectric material.

Keyword: ferroelectric catalysis

Yaqiong Wang, Man Zhang, Jianguo Liu, Haibin Zhang, Feng Li, Chiao-Wei Tseng, Bin Yang, Graham Smith, Jiwei Zhai, Zhen Zhang, Steve Dunn*, Haixue Yan*

Domain wall free polar structure enhanced photodegradation activity in nanoscale ferroelectric $Ba_xSr_{1-x}TiO_3$

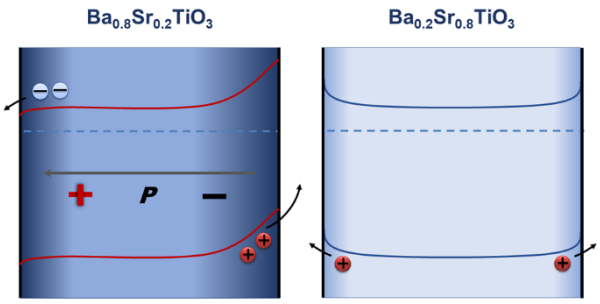

Supporting Information

Domain wall free polar structure enhanced photodegradation activity in nanoscale ferroelectric $Ba_xSr_{1-x}TiO_3$

Yaqiong Wang, Man Zhang, Jianguo Liu, Haibin Zhang, Feng Li, Chiao-Wei Tseng, Bin Yang, Graham Smith, Jiwei Zhai, Zhen Zhang, Steve Dunn, Haixue Yan**

1. Supplementary Figures

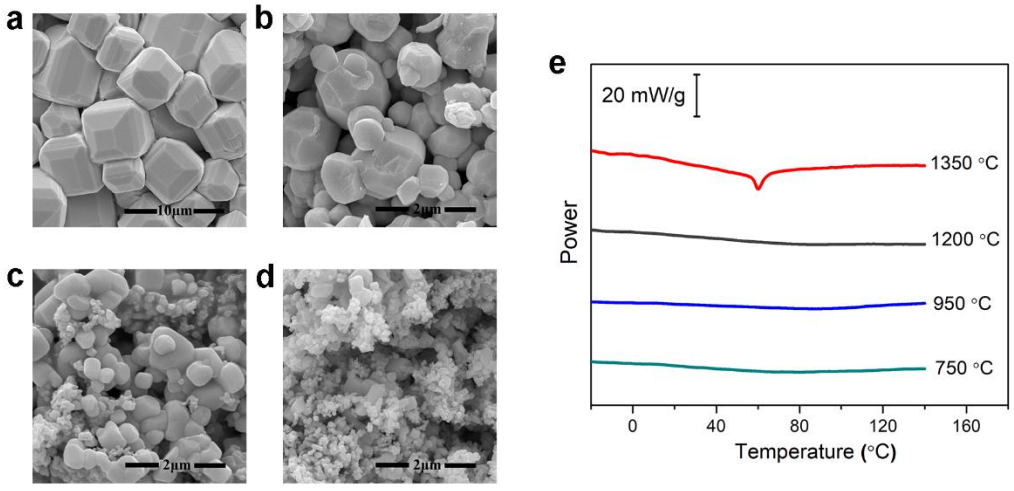

Figure S1. Characterisation of the polar structure dependence of $Ba_{0.8}Sr_{0.2}TiO_3$ powders on grain size and temperature. a, b, c, d, SEM images of $Ba_{0.8}Sr_{0.2}TiO_3$ (possessed at 750 °C) post-annealed at 1350 °C, 1200 °C, 950 °C and 750 °C, respectively. e, DSC data for $Ba_{0.8}Sr_{0.2}TiO_3$ samples processed with increasing temperatures.

To study the dependence of polar structure on grain size, $Ba_{0.8}Sr_{0.2}TiO_3$ powders of different grain sizes were obtained by post-annealing the $Ba_{0.8}Sr_{0.2}TiO_3$ powders (possessed at 750 °C) at different temperatures. The $Ba_{0.8}Sr_{0.2}TiO_3$ samples were post-annealed at 950 °C, 1200 °C and 1350 °C for 10 hours, respectively. Figure S1 a,b,c,d show SEM images of the as-obtained samples. It can be seen from the figures that the $Ba_{0.8}Sr_{0.2}TiO_3$ grain sizes increase dramatically with annealing temperature ranging from 750 °C to 1350 °C. Though large grains with a sub-

micro/micro size can be observed in all four samples, it is obvious that ultrafine grains with size smaller than 100 nm are dominating in the 750 °C sample and larger grains subsequently become the majority with increasing temperature, with micro-grains obtained in the 1350 °C sample. DSC measurement was conducted to check the dependence of phase transition thermal characteristics of the $Ba_{0.8}Sr_{0.2}TiO_3$ samples processed at different temperatures. Figure S1e gives DSC data for $Ba_{0.8}Sr_{0.2}TiO_3$ samples. It can be seen that the endothermic feature near 60 °C which is attributed to the tetragonal-cubic transformation is only observed in the sample post-annealed at 1350 °C. With decreased post-annealing temperatures, the endothermic peak disappeared, which is analogous to the phenomenon observed by M. H. Frey *et al*.[1] in the study of $BaTiO_3$ particles processed in different temperatures. This has been suggested to result from the single-domain feature by M. H. Frey *et al*. In their study, $BaTiO_3$ particles of different grain sizes exhibited multi-single domain transformation at the size of ~ 400 nm, demonstrated by the hot-stage TEM and DSC characterisations. Thus, it can be suggested that the $Ba_{0.8}Sr_{0.2}TiO_3$ sample annealed at 750 °C has a single-domain-single-grain structure. We show Raman spectra in Fig S2 indicating the transition to a non-polar material for the $Ba_{0.8}Sr_{0.2}TiO_3$ material as it passes through the Curie point. In order to determine the influence of the variation in the valance band position for the two different materials we have completed X-ray Photoelectron Spectroscopy (XPS) analysis for the two samples. The results are shown in Fig S3 and indicate that there is negligible change to the oxidation potential in the valence band for both materials. There are small changes to the fine detail of the band structure that are due to the defect states within the materials.

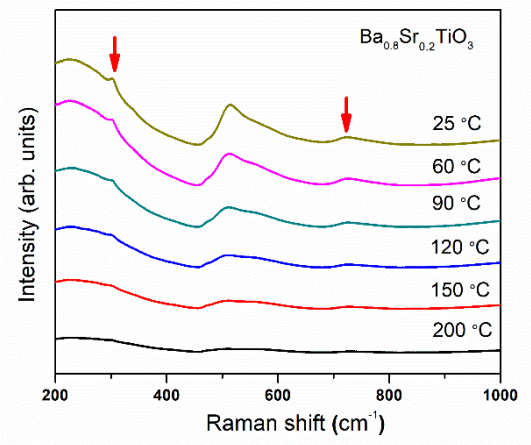

Figure S2. Raman spectra of $Ba_{0.8}Sr_{0.2}TiO_3$ at different temperatures. Raman spectra of the $Ba_{0.8}Sr_{0.2}TiO_3$ sample (processed at 750 °C) collected over a range of temperatures between 25 °C and 200 °C have been obtained to reveal its phase transformation with temperature changing through the Curie point. With increasing temperature, the two peaks (at 302 cm^{-1} and 722 cm^{-1}) exhibit larger linewidths, indicating that the tetragonality is accompanied by a decreased structural coherence[2]. And the two peaks gradually vanish when the temperature increases from 25 °C to 90 °C, demonstrating a tetragonal to cubic phase transition.

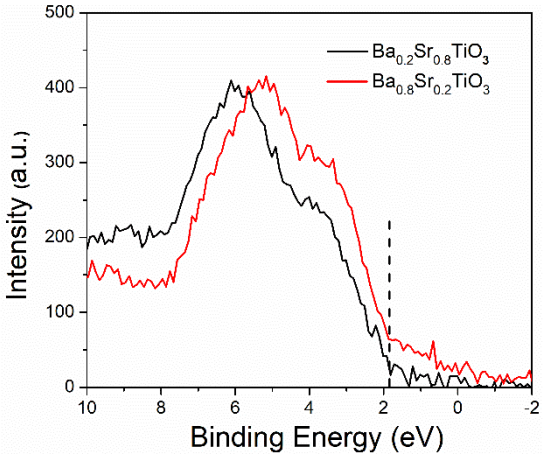

Figure S3. X-Ray Photoelectron Spectroscopy (XPS) valence band spectra of $Ba_{0.8}Sr_{0.2}TiO_3$ and $Ba_{0.2}Sr_{0.8}TiO_3$ that indicates negligible change in the oxidation potential for a hole in both materials. There are some small changes to the fine detail of the band structure with the differences being associated with defect states.

2. Supplementary Tables

Table S1. Particle Size and Surface Area of $Ba_{0.8}Sr_{0.2}TiO_3$ and $Ba_{0.2}Sr_{0.8}TiO_3$

Sample	Average particle size (nm, SEM)	BET surface area (m^2/g)
$Ba_{0.8}Sr_{0.2}TiO_3$	70.8	7.3904
$Ba_{0.2}Sr_{0.8}TiO_3$	65.2	7.9646

3. Supplementary Methods

Sample preparation

Barium strontium titanite nanocrystals were prepared by molten-salt synthesis (MSS) method. Barium oxalate (99.999%), Strontium oxalate (95%), Sodium chloride (99.0%) and Potassium chloride (99%) were obtained from Alfa Aesar and used as received. Titanium dioxide (nanopowder, 21 nm primary particle size, ≥99.5%) were obtained from Sigma-Aldrich and used as received. In a typical synthesis procedure of $Ba_{0.8}Sr_{0.2}TiO_3$, 0.08 mol of BaC_2O_4 and 0.02 mol SrC_2O_4 along with 2 mol NaCl and 2 mol KCl were added to a PTFE pot and mixed thoroughly by ball milling for 4 h using ethanol and zirconia balls. The obtained slurry was dried out at 100 °C overnight. The processed mixture was placed in a ceramic crucible, heated at a ramp rate of 5 °C /min to an annealing temperature at 750 °C for 1 h, and cooled thereafter to room temperature within the furnace. Samples were subsequently washed several times with hot distilled water and filtered by vacuum suction. The as-prepared powders were collected and dried at 80 °C in an oven overnight. Preparation of $Ba_{0.2}Sr_{0.8}TiO_3$ powders was employed using different molar ratios of the initial precursors. $Ba_{0.8}Sr_{0.2}TiO_3$ samples prepared at 750 °C were post-annealed at 950 °C, 1200 °C and 1350 °C to investigate the effect of grain size on the domain structure. The post-annealing treatments were conducted by heating the $Ba_{0.8}Sr_{0.2}TiO_3$ samples up to the desired temperatures by a rate of 10 °C/min and held for 10 hours, followed by cooling down in a rate of 5 °C/min. If not noticed specifically, the $Ba_{0.8}Sr_{0.2}TiO_3$ samples mentioned in the paper refer to the original samples processed at 750 °C.

Characterisation

X-ray diffraction (XRD) patterns of the powders were obtained with a Panalytical Xpert Pro diffractometer using Cu Ka radiation. The morphology of the powders was observed using a scanning electron microscope (SEM, FEI Inspect F) and a transmission electron microscope (TEM, FEI Titan Themis (200 kV)). Optical absorption of the obtained BST powders was measured using a PerkinElmer Lambda 950 UV-vis spectrophotometer. X-Ray Photoelectron Spectroscopy (XPS) was performed to determine the valence band maximum of the two BST samples. The XPS is a bespoke system with Specs GmbH Phoibos 150 mm 9-channeltron analyser. The valence band spectra were acquired with 20 eV pass energy and 0.1 eV energy

steps using a VG Microtech twin-anode Al K-alpha source. Temperature dependent Raman spectra were acquired by Raman scattering spectrometer (Horiba Jobin-Yvon HR800, France) with a 532 nm wavelength laser and was equipped with a Linkam THMSE 600 heating stage. Thermal properties of the materials were analyzed using a differential scanning calorimeter (DSC) (DSC822e, Mettler-Toledo, OH, USA) under a N_2 atmosphere.

Photocatalytic activity of the catalysts was evaluated through decolorization of Rhodamine B (Rh B, Sigma, 99.99%) dye solution. In a typical procedure, 0.15 g catalyst powder was mixed with 50 ml of 10 ppm dye solution in a Petri dish. After kept in dark for 30 min under constant stirring, the mixture was placed under a solar simulator (Newport). Irradiation intensity of the simulator was fixed at 1 sun (100 mW/cm^2) using a silicon reference cell. A 2 ml solution sample was taken at fixed intervals of 30 min, followed by centrifugation at 10000 rpm for 15 min to remove the catalyst powder. Optical absorption of the obtained dye solution was measured by UV-vis spectrophotometer.

[1] M. H. Frey, D. A. Payne, *Phys. Rev. B* **1996**, *54*, 3158.

[2] M. B. Smith, K. Page, T. Siegrist, P. L. Redmond, E. C. Walter, R. Seshadri, L. E. Brus, M. L. Steigerwald, *J. Am. Chem. Soc.* **2008**, *130*, 6955.